WIND TUNNEL TEST OF AN ANTI-ICING APPROACH BY HEAT PIPE FOR WIND TURBINE BLADES UNDER THE RIME ICE CONDITION

by

Xiao-Juan LI[a], Wen-Feng GUO[a], Yan LI[a*], Zhi XU[a], and Fang FENG[b]

[a] Engineering College, Northeast Agricultural University, Harbin, China
[b] College of Science, Northeast Agricultural University, Harbin, China

Original scientific paper
https://doi.org/10.2298/TSCI2106485L

The icing events for the wind turbine blade is the key problem in the low temperature conditions. Heating is considered to be the most efficient approach to prevent from the ice formation on the turbine blade surface. However, this kind of method consumes a certain amount of energy. In this present study, an anti-icing method, using the heat pipe technology, is proposed to prevent from icing on the blade surface, and the anti-icing energy is from the waste heat generated during the operation of a wind turbine, which can reduce the assumption of the energy. The researches on the anti-icing temperature characteristics of the test model, based on the heat pipe anti-icing method, are carried out in an icing wind tunnel combining with the low natural temperature. The effects of the wind speed and heat source temperature on the heat transfer of heat pipes are investigated. The icing distribution and the temperature change of the anti-icing process of an airfoil with NACA0018 are explored, and the variation of the icing thickness of the airfoil with icing time, under the different heat source temperature conditions, is analyzed. The results indicate that the blade surface temperature, which is lower than 0 °C, is more beneficial to the heat transfer of the heat pipe, and the ice prevention, based on the heat transfer of the heat pipe, can achieve a better anti-icing effect.

Key words: *wind turbine, anti-icing, rime ice, heat pipe, wind tunnel test*

Introduction

In recent years, wind turbines in cold areas are encountering increasingly severe tests. The wind turbine blades, cabins, and shrouds would be frozen when the ambient temperature is lower than 0 °C and there is water vapor. Since the blade is the main working component of a wind turbine, icing would seriously affect its aerodynamic performance and load distribution, resulting in a decrease in wind turbine power generation efficiency and work instability, and even safety accidents. Therefore, it is developing effective solutions to mitigate wind turbine icing is highly desirable and urgent.

Researchers worldwide have conducted a lot of research on the mechanism and hazards of wind turbine icing [1-5]. Different methods of anti-icing and deicing have been developed and studied to reduce the harm of icing, including coating, mechanical, and heating methods [6-8]. Specifically, heating methods keep the blade surface temperature above 0 °C to prevent the blade from freezing, including hot air injection, resistive heating, microwave heating, infrared heating, and plasma heating [9-12]. It is of more practical significance to re-

[*] Corresponding author, e-mail: liyanneau@163.com

duce the energy consumed in the process of anti-deicing because the aforementioned heating methods need to consume additional energy to prevent and remove ice on the blades [13-16]. Besides, a heat pipe is a kind of efficient heat transfer element. Its thermal conductivity range is 103-104 W/mk. In the process of operation, the wind turbine will produce energy loss in the form of waste heat. The loss of a transmission system is usually 5% of the output power of the wind turbine. The main heating components of a wind turbine are generator and gearbox, as well as power conversion electronic components and transformers. All of these heat-generating components need to be actively cooled to maintain the normal operation.

This paper presents a new method to prevent ice accretion on the blades using the excess heat energy generated during the operation of a wind turbine. The wind tunnel test of a blade with a heat pipe was performed under natural low temperature conditions. The waste heat source of the wind turbine was simulated using a constant temperature water bath pot. Besides, the effects of heat pipe heat transfer on the blade surface and water bath temperature under icing and non-icing conditions were compared. Moreover, the changes in blade surface temperature and icing state under different heat source temperatures were collected. Finally, the optimum heat source temperature of blade anti-icing was obtained by prolonging the running time and collecting the icing state of the blade at different time periods.

The theory of heat pipes

The heat pipe theory used in this paper was proposed by Cotter, and the equations related are given [17].

In the any position of heat pipe in axial, the pressure difference at the vapor-liquid interface is given:

$$p_{\mathrm{v}}(x)-p_{\mathrm{l}}(x)=\frac{2\sigma\cos\theta}{r_c} \tag{1}$$

where $p_{\mathrm{v}}(x)$ and $p_{\mathrm{l}}(x)$ are the pressures of the vapor and the liquid, respectively, σ – the surface tension of the liquid, θ – the contact angle or infiltration angle, and r_c – the radius of the meniscus at the vapor-liquid interface.

The flow pressure drop of the liquid in the wick is given:

$$\frac{\mathrm{d}p_{\mathrm{l}}}{\mathrm{d}x}=\rho_{\mathrm{l}}\mathrm{g}\sin\varphi-\frac{b\mu_{\mathrm{l}}\dot{m}_{\mathrm{l}}(x)}{\pi\left(r_{\mathrm{w}}^2-r_{\mathrm{v}}^2\right)\varepsilon r_{\mathrm{hl}}^2\rho_{\mathrm{l}}} \tag{2}$$

where ρ_{l} is the density of the liquid, g – the acceleration of gravity, φ – the inclination angle between the heat pipe and the horizontal plane, μ_{l} – the viscosity of the liquid, $\dot{m}_{\mathrm{l}}(x)$ – the mass-flow rate of the liquid, b – the dimensionless constant for correcting the curvature of the capillary with the range of variation and it is equally to 10-20, r_{w} and r_{v} – the hydraulic radius of the wick and steam space, respectively, r_{hl} – the effective hydraulic radius of the wick, and ε – the ratio between the void volume and the total volume of the wick.

Without the impact caused by dynamic pressure changes, the flow pressure drop of the vapor is given:

$$\frac{\mathrm{d}p_{\mathrm{v}}}{\mathrm{d}x}=-\frac{8\mu_{\mathrm{v}}\dot{m}_{\mathrm{v}}}{\pi\rho_{\mathrm{v}}r_{\mathrm{v}}^4}\left(1+\frac{3}{4}\mathrm{Re}_r-\frac{11}{270}\mathrm{Re}_r^2+\ldots\right),\ \left|\mathrm{Re}_r\right|\ll 1 \tag{3}$$

$$\frac{\mathrm{d}p_{\mathrm{v}}}{\mathrm{d}x}=-\frac{S\dot{m}_{\mathrm{v}}}{4\rho_{\mathrm{v}}r_{\mathrm{v}}^4}\frac{\mathrm{d}\dot{m}}{\mathrm{d}x},\ \left|\mathrm{Re}_r\right|\to\infty \tag{4}$$

and

$$\frac{\mathrm{d}p_\mathrm{v}}{\mathrm{d}x}=-\frac{0.0665\mu_\mathrm{v}^2}{\rho_\mathrm{v}r_\mathrm{v}^3}\mathrm{Re}^{7/4},\ \ \mathrm{Re}_r\approx 0,\ \ \mathrm{Re}>1000 \tag{5}$$

where Re_r and Re is the radial Reynolds number and the axial Reynolds number, respectively, μ_v – the viscosity, ρ_v – the density, $\dot{m}_\mathrm{v}$ – the mass-flow of steam, and S – the coefficient.

The function of the pressure difference and the mass-flow at the vapor-liquid interface is given:

$$-\frac{\mathrm{d}\dot{m}_\mathrm{v}}{\mathrm{d}x}=\frac{\mathrm{d}\dot{m}_\mathrm{l}}{\mathrm{d}x}=\frac{\alpha r_\mathrm{v}(p_\mathrm{vc}-p_\mathrm{sc})}{\sqrt{\dfrac{\mathrm{R}_0T}{2\pi m}}} \tag{6}$$

where p_vc and p_sc are the pressure on the interface of the vapor and the liquid, respectively, α – the correction coefficient which close to 1, R_0 – the universal gas constant, T – the temperature of gas, and m – the molecular weight of steam.

The function of heat transfer quantity and mass-flow in axial is given:

$$Q(x)=h_{fg}\dot{m}_\mathrm{v}(x) \tag{7}$$

where h_{fg} is the evaporation heat of the liquid.

The heat among the unit length is given:

$$\frac{\mathrm{d}Q(x)}{\mathrm{d}x}=H(x,T_\mathrm{p},Q) \tag{8}$$

where x is the length of the heat pipe, T_p – the temperature of the outer wall of the heat pipe, and Q – is the heat transfer quantity in axial.

The T_p is given:

$$T_\mathrm{p}=T_\mathrm{v}+\frac{H}{k} \tag{9}$$

where T_v is the temperature at the vapor-liquid interface and k – the composite thermal conductivity of the tube wall and the wick.

Test model and experimental set-up

Test model

The blade used in the test is a NACA 0018 airfoil, which has an acceptable aerodynamic and structural performance. The symmetrical airfoil was chosen because it can analyze the heat transfer characteristics between the heat pipe and the airfoil more clearly. Besides, aluminum commonly used in aircraft wing research models was selected as the model material. Aluminum has stable thermal conductivity while the composition of glass fiber reinforced plastic material is complex and diverse. Thus, it is not convenient for basic research. Then, an aluminum blade model with a surface roughness of 3.2 μm was selected to explore the general law of heat pipes used in airfoils. As shown in fig. 1, the turbine blade model has an airfoil chord

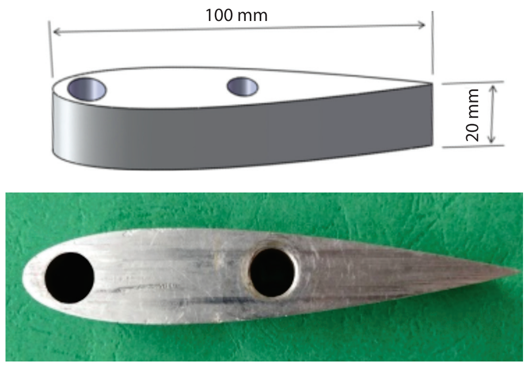

Figure 1. Test blade

length of 100 mm (*i.e.*, C = 100 mm) and a spanwise length of 20 mm, fitting nicely into the test section of the wind tunnel system.

Heat pipe

A sintered heat pipe with a specification diameter Φ of 6 mm was selected in the experiment. Considering that the temperature of the experimental environment was lower than 0 °C and the temperature range of the heat source at the evaporation end of the heat pipe was 0-100 °C, a low temperature heat pipe with ethanol was selected as the working medium. As shown in fig. 2, there are invalid ends at both ends of the heat pipe, there are spinning seals and vacuum exhaust seals at both ends of the sintered heat pipe in the production process, and the end of the heat pipe after shrinkage cannot have the same effective heat transfer area as the other parts. The specific parameters are listed in tab. 1.

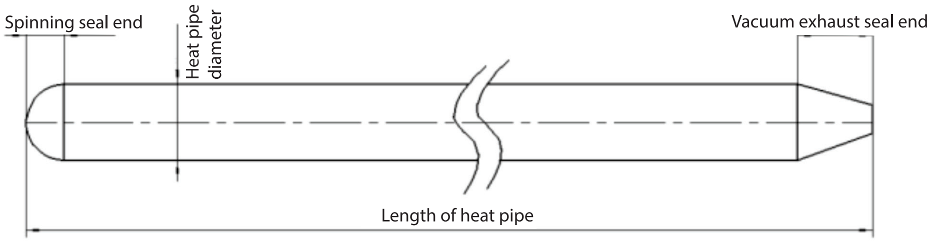

Figure 2. Heat pipe structure drawing

Table 1. Heat pipe parameters

Specifications	Working medium	Main material	Diameter, Φ	Length, L	Wall thickness	Spinning seal end length	Vacuum exhaust seal end length
Diameter of 6 sintered heat pipe	Ethanol	C1020 copper	6 mm	500 mm	0.3 mm	3 mm	6-7 mm

Temperature measurement

As shown in fig. 3, the center of the heat pipe at the top of the model was set to the x-axis, y-axis, and z-axis along the chord length, thickness, and spanwise directions, respectively. The temperatures of four Points (A, B, C, D) marked in fig. 3 were probed for detailed analysis. The four points were arranged on the blade surface as follows. Point A was located in the center of the leading edge of the blade, the angle between the x-axis and the line connecting the origin and Point A and Point B was 45° and 90°, respectively. Point D was symmetrical to Point C with respect to the x-axis. The spanwise direction of the four points was located at the condensation and exothermic end of the heat pipe and at the top 8 mm of the blade. The temperature was measured by a K-type alloy thermocouple with a wire diameter of 0.25 mm and a solder joint diameter of 0.8 mm.

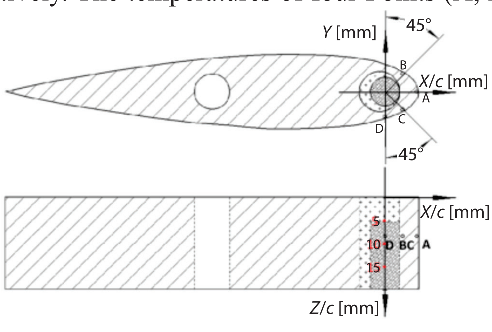

Figure 3. Positions of temperature measuring points

Experimental system arrangement

It can be shown in fig. 4 that the experimental system includes a wind tunnel, heating device, data acquisition device, and a fixing device. The length and width of the wind tunnel are 9.1 m and 2.3 m, respectively and the size of the air outlet is 1 m × 1 m. The blade model was fixed on the fixing frame, and the condensation end of the heat pipe was fixed in the drill hole at the front end of the blade. Besides, heat conduction silica gel was coated on the front side of the drill hole to enhance heat transfer on the front side of the blade, and rubber-plastic insulation material was adopted on the backside to prevent heat transfer from the heat pipe to the backside. Moreover, the insulated section of the heat pipe was wrapped in rubber-plastic insulation material. The evaporating end of the heat pipe was connected to the water bath. Furthermore, the temperature of the heat source (heat storage device for storing waste heat) was simulated by setting different temperatures of the water bath. The water bath has a heating power of 800 W, with a temperature sensor and a temperature control device. The temperature range was 5-100 °C. The error of temperature control was ±1 °C. The test was conducted in a natural low temperature environment. The parameters of working conditions are listed in tab. 2.

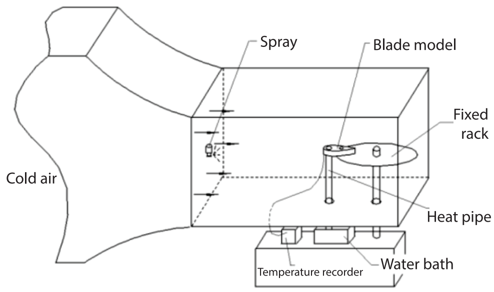

Figure 4. Test system

Table 2. Working condition parameters

Working condition	Wind speed [ms^{-1}]	Wind tunnel center temperature [°C]	Setting temperature of the heat source [°C]	Temperature measuring point
1	0	11 ±1	25, 30, 40, 50, 60, 70	A
2	4	–6 ±1	25, 30, 40, 50, 60, 70	A
3	4	–6 ±1	25, 30, 35, 40, 45, 50, 55, 60, 65, 70	A, B, C, D
4	4	–6 ±1	10, 20, 30, 40, 50	*n*/*a*

Results and analysis

Anti-icing performance of heat pipe under icing and non-icing conditions

The temperature changes of heat source and blade Point A under working Condition 1 (μ = 0 m/s, the center temperature of wind tunnel is 11 °C) and Condition 2 (μ = 4 m/s, the center temperature of wind tunnel is –6 °C) were recorded to compare the anti-icing effect of the heat pipe under icing and non-icing conditions. After the heat source temperature was set, they operated for the same time. The heat source temperature was set at 25 °C, 30 °C, 40 °C, 50 °C, 60 °C, and 70 °C. The wind tunnel was preheated for at least 30 minutes to ensure that the heat balance reached in the center of the wind tunnel. When the temperature of the heat source reached 25 °C, the sprinkler system was turned on, and the time was set to t = 0 second.

The temperature changes of Point A and heat source under the two working conditions show different trends, as shown in fig. 5. The temperature at Point A of working Condition 1 has the same trend as its heat source temperature, increasing with the increased heat source temperature. The temperature at Point A of working Condition 2 first decreased and then increased

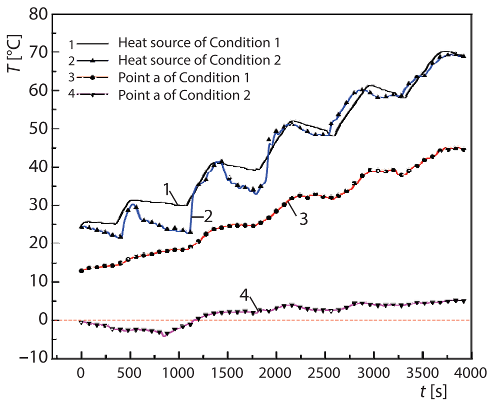

Figure 5. Temperature of the heat source and blade surface under working Conditions 1 and 2

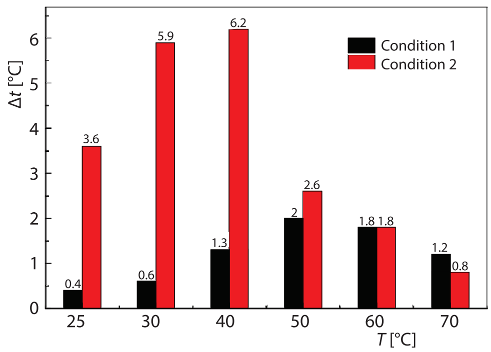

Figure 6. Temperature difference of heat source within 5 minutes

slowly, much lower than that of working Condition 1. This was because the large heat transfer on the surface of the blade under working Condition 2 could result in freezing on the surface. After the temperature of the two heat sources reached the set temperature, they both showed a downward trend. After the temperature was set to 25 °C, 30 °C, and 40 °C, the decreasing trend of the heat source temperature in working condition two was obviously larger than that in working condition 1, and the temperature difference before and after was larger. Besides, after the temperature was set to 50 °C, 60 °C, and 70 °C, the trend was similar to that of working condition 1: the difference decreased gradually with the slight decreasing temperature.

The details of the variation of temperature difference of the heat source under the two working conditions are shown in fig. 6. The temperature difference reached the maximum and the heat dissipation of the heat source was the most when the heat source temperature was 50 °C in working Condition 1 and 40 °C in working Condition 2. The temperature difference of working Condition 2 was larger at 25 °C, 30 °C, and 40 °C, and decreased gradually at 50 °C, 60 °C, and 70 °C, similar to working Condition 1. This may be because the larger the temperature difference between the two ends of the heat pipe, the greater the heat conduction power of the heat pipe under working Condition 2. The results revealed that it is more beneficial to heat pipe heat transfer when the blade surface temperature is lower than 0 °C.

Anti-icing performance of heat pipe at different heat source temperatures

Under the condition of working Condition 3 (μ = 4 m/s, wind tunnel center temperature is –6 °C), the heat source temperature was set in the range from 20-70 °C with an interval of 5 °C to further investigate the anti-icing performance of the heat pipe at different heat source temperatures. Since there was a certain deviation between the set value and the actual value, the actual heat source temperature is presented in the figure. After the wind tunnel was preheated, the sprinkler system was turned on when the heat source temperature reached 20 °C.

Figure 7 shows that the temperature of the measuring point varied with the heat source temperature under working Condition 3. With the increasing heat source setting temperature, the blade surface temperature first decreased and then increased. The temperature decline rate of each point on the blade surface was different, and the temperature of Point D decreased the fastest. Besides, the temperature of each point tended to be the same when the blade temperature approached 0 °C. Meanwhile, the temperature of each point fluctuated up and down as the temperature increased. After the heat source temperature reached 60 °C, the temperature of each point of the blade tended to be stable. Specifically, the temperature of Points B and C was similar and the highest, the temperature of Point A was in the middle, and the temperature of Point D was the lowest. After the heat source temperature reached 35 °C, the blade surface temperature rose to more than 0 °C. The analysis demonstrated that the blade surface temperature was lower than 0 °C when the heat source temperature was low, exhibiting a downward trend, meanwhile, the phenomenon of icing occurred. Additionally, when the heat source temperature reached 30 °C, the blade surface temperature increased and the ice appeared to melt gradually and when the heat source temperature reached 35 °C, the blade surface temperature was more than 0 °C with a downward trend and when the heat source temperature reached 40 °C, the blade surface temperature can be maintained above 0 °C.

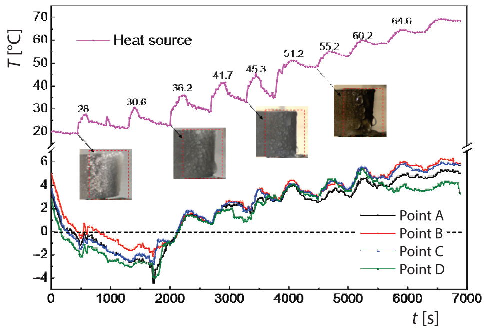

Figure 7. Temperature changes with time and the anti-icing state of blade surface under Condition 3

Icing thickness and icing state

Under the working Condition 4 (μ = 4 m/s, the central temperature of wind tunnel is –6 °C), the heat source temperature was set in the range of 10-50 °C with an interval of 10 °C to investigate the ice thickness and icing state in the process of dynamic ice accretion. After the temperature was set, photos of ice accretion were recorded at 5, 10, and 15 minutes. The ice thickness at different heat source temperatures at different times was shown in fig. 8. With increasing heat source temperature, the ice thickness became smaller and small-

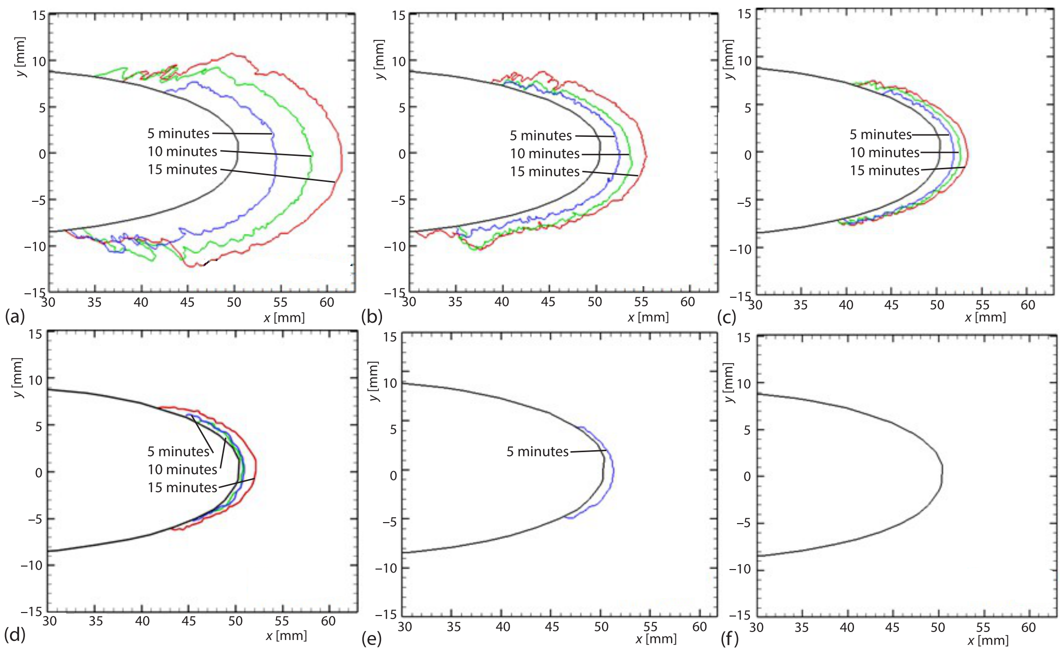

Figure 8. Ice thickness and icing state at different heat source temperatures; (a) non-heating, (b) T = 10 °C, (c) T = 20 °C, (d) T = 30 °C, (e) T = 40 °C, and (f) T = 50 °C

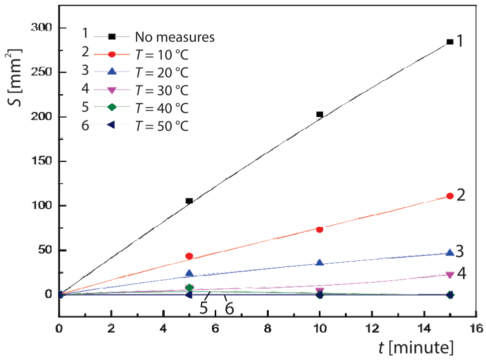

Figure 9. Icing cross-sectional area at different heat source temperatures

er, and the icing range shrank to the center of the leading edge of the blade. The heating of the blade surface by the heat pipe delayed the icing. Besides, the higher the heat source temperature, the better the anti-icing effect.

The variation of the cross-sectional area of heat pipe ice accretion at the different heat source temperatures is shown in fig. 9. The cross-sectional area of ice accretion accumulated approximately linearly. When the heat source temperature reached 40 °C and 50 °C, the cross-sectional area of icing approached 0, and there was no ice accretion over the blade surface.

Conclusion

To sum up, the higher the temperature of the heat source, the higher the surface temperature of the blade. Moreover, the surface temperature of the blade can be maintained above 0 °C when the heat source temperature (the evaporator temperature of the heat pipe) is higher than 40 °C, having a better effect for preventing ice formation.

Acknowledgment

This research was supported by the National Natural Science Foundation of China (NSFC) [Grant No. 51976029].

Nomenclature

b – dimensionless constant
h_{fg} – latent heat, [Jmol^{-1}]
k – thermal conductivity, [Wm^{-1}K^{-1}]
L – length, [mm]
m – molecular weight, [kg]
$\dot{m}$ – mass-flow, [kgs^{-1}]
p – pressure, [Pa]
Q – heat, [J]
R_0 – gas constant
Re – Reynolds number
r – radius, [mm]
S – coefficient
T – temperature, [°C]
t – time, [s]

Greek symbols

ε – ratio
θ, φ – angle, [°]
μ – viscosity, [ms^{-1}]
ρ – density, [kgm^{-3}]
σ – surface tension, [Nm^{-1}]
Φ – diameter, [mm]

References

[1] Li, Y., *et al.*, Aerodynamic Characteristics of Straight-Bladed Vertical Axis Wind Turbine with a Curved-Outline Wind Gathering Device, *Energy Conversion and Management*, *203* (2020), 1, pp. 112249.1-112249
[2] Li, Y., *et al.*, A Wind Tunnel Experimental Study of Icing on Wind Turbine Blade Airfoil, *Energy Conversion and Management*, *85* (2014), 7, pp. 591-595
[3] Li, Y., *et al.*, Icing Distribution of Rotating Blade of Horizontal Axis Wind Turbine Based on Quasi-3-D Numerical Simulation, *Thermal Science*, *22* (2018), 2, pp. 681-691
[4] Shu, L. C., *et al.*, Numerical and Experimental Investigation of Threshold De-Icing Heat Flux of Wind Turbine, *Journal of Wind Engineering and Industrial Aerodynamics*, *174* (2018), Mar., pp. 296-302
[5] Guo, W. F., *et al.*, Wind Tunnel Tests of the Rime Icing Characteristics of a Straight-Bladed Vertical Axis Wind Turbine, *Renewable Energy*, *179* (2021), Dec., pp. 116-132

[6] Fakorede, O., *et al*., Ice Protection Systems for Wind Turbines in Cold Climate: Characteristics, Comparisons and Analysis, *Renewable and Sustainable Energy Reviews*, *65* (2016), Nov., pp. 662-675
[7] Wang, Y. B., *et al*., Progress on Ultrasonic Guided Waves De-Icing Techniques in Improving Aviation Energy Efficiency, *Renewable and Sustainable Energy Reviews*, *79* (2017), Nov., pp. 638-645
[8] Wang, T., *et al*., Passive Anti-Icing and Active Deicing Films, *ACS Applied Materials & Interfaces*, *8* (2016), 22, pp. 14169-14173
[9] Vertuccio, L., *et al*., Effective De-Icing Skin Using Graphene-Based Flexible Heater, *Composites Part B*, *Engineering*, *162* (2019), Apr., pp. 600-610
[10] Akhtar, N., *et al*., Fluorinated Graphene Provides Long Lasting Ice Inhibition in High Humidity, *Carbon*, *141* (2019), 1, pp. 451-456
[11] Yao, X., *et al*., An Advanced Anti-Icing/De-Icing System Utilizing Highly Aligned Carbon Nanotube Webs, *Carbon*, *136* (2018), 2, pp. 130-138
[12] Cheng, T., *et al.*, Magnetic Particle-Based Super-Hydrophobic Coatings with Excellent Anti-Icing and Thermoresponsive Deicing Performance, *Journal of Materials Chemistry A*, *3* (2015), 43, pp. 21637-21646
[13] Gao, L. Y., *et al*., A Hybrid Strategy Combining Minimized Leading-Edge Electric-Heating and Superhydro-Ice-Phobic Surface Coating for Wind Turbine Icing Mitigation, *Renewable Energy*, *140* (2019), 4, pp. 943-956
[14] Jiang, G., *et al*., Superhydrophobic SiC/CNT Coatings with Photo-Thermal Deicing and Passive Anti-Icing Properties, *ACS Applied Materials & Interfaces*, *10* (2018), 42, pp. 36505-36511
[15] Wei, B., *et al*., The SDBD Based Plasma Anti-Icing: A Stream-Wise Plasma Heat Knife Configuration and Criteria Energy Analysis, *International Journal of Heat and Mass Transfer*, *138* (2019), 12, pp. 163-172
[16] Liu, Y., *et al.*, An Experimental Study on the Thermal Effects of Duty-Cycled Plasma Actuation Pertinent to Aircraft Icing Mitigation, *International Journal of Heat and Mass Transfer*, *136* (2019), 3, pp. 864-876
[17] Zhuang, J., *et al*., *Heat Pipe and Heat Pipe Exchanger* (in Chinese), Shanghai Jiao Tong University, Shanghai, China, 1989

Paper submitted: April 5, 2021
Paper revised: June 13, 2021
Paper accepted: July 12, 2021